Journal of Applied Fluid Mechanics, Vol. 15, No. 3, pp. 767-780, 2022.
Available online at www.jafmonline.net, ISSN 1735-3572, EISSN 1735-3645.
https://doi.org/10.47176/jafm.15.03.32914

Numerical Investigation on the Effect of Leading-Edge Tubercles on the Laminar Separation Bubble

A. Sathyabhama[1†] and B. K. Sreejith[2]

[1] *Department of Mechanical Engineering, National Institute of Technology Karnataka, Mangaluru, Karnataka, India-575025, India*
[2] *Department of Mechanical Engineering, AJ Institute of Engineering and Technology, Mangaluru, Karnataka, India-575006, India*

† *Corresponding Author Email*: *bhama72@gmail.com*

(Received April 22, 2021; accepted November 12, 2021)

ABSTRACT

The effect of leading-edge tubercles on the aerodynamic performance of E216 airfoil is studied by steady 3D numerical simulations using Transition $\gamma-Re_\theta$ turbulance model. The investigation is carried out for the various angles of attack in the pre-stall region at Reynolds number of 100,000. Various tubercle configurations with different combinations of amplitude ranging from 2 mm to 8 mm and wavelength varying from 15.5mm to 62 mm are studied. The effect of tubercle parameters on the laminar separation bubble (LSB) is extensively studied. Improvement in the coefficient of lift (C_l) is observed for most of the tubercled models and is significant at high angles of attack. But the simultaneous increase in the drag coefficient resulted in a marginal improvement in the coefficient of lift to drag ratio (C_l/C_d) for most of the cases except for A2W62, which produced a peak value of 46.91 at AOA 6° which is higher than that for the baseline by 7.37%. Compared to the baseline, the magnitude of suction peak is higher along the trough and lower along the peak. The low amplitude and low wavelength tubercle model exhibited smooth surface pressure coefficient (C_p) distribution without any sign of strong LSB formation. The LSB moves upstream with the increase in amplitude and wavelength. The LSB along the trough is formed ahead of that at peak inducing three-dimensional wavy shaped LSB unlike the straight LSB as in baseline. Two pairs of counter rotating vortices are formed on the airfoil surface between the adjacent peaks at two different chord-wise locations which strongly alter the flow pattern over it.

Keywords: Airfoil; Laminar separation bubble; Small scale wind turbine; Tubercle; Turbulent flow.

NOMENCLATURE

A	amplitude of oscillation	F_y	Y component of the resultant pressure force acting on the lower side
a	cylinder diameter	f, g	generic functions
C_μ	pressure coefficient	h	height
C_X	force coefficient in the x direction	i	time index during navigation
C_Y	force coefficient in the y direction	j	space index
c	chord	α	angle of attack
dt	time step	γ	dummy variable
F_x	X component of the resultant pressure force		

1. INTRODUCTION

The exponential growth of energy demand worldwide leads to the generation of energy from all possible sources. Small-scale wind turbines (SSWT) are such an alternative, and as a result, there has been increased performance-based research in the SSWT field in recent years. Due to many aerodynamical reasons, the airfoils of such turbines are exposed to low Reynolds number (Re) conditions ($10^4 \le \mathrm{Re} \le 10^5$ (Musial and Cromack 1988)). The airfoil sections of SSWT blades thus suffer from the severe stall and laminar separation bubble (LSB) at a low angle of attack (AOA). Controlling the formation and extent of the LSB is essential to improve the performance of the low Re airfoils. This can be achieved by the premature transition of flow into turbulence with the help of cost effective passive flow control methods like wires, grits, dimples and boundary layer trips (BLT) (Genc *et al.* 2012). Passive flow control techniques achieved by geometrical modification of airfoils without drag penalty are most acceptable for wind turbine applications due to less complexity compared to active flow control

methods. Incorporating undulations, called tubercles, on airfoil leading edge is one of the recent passive flow control techniques to improve the airfoil performance. These tubercles resemble the protuberance found over humpback whale flippers, as shown in Fig. 1. The observations show that the humpback whale's high maneuverability is due to the tubercles on the leading edge of its flippers (Bushnell and Moore 1991).

Two types of studies are reported in the literature on the effects of leading-edge tubercles on the aerodynamic performance, depending on the models used, namely, airfoil studies (two-dimensional and wing studies (three-dimensional). Tubercles improved the performance of airfoil only in the post-stall region as per the investigations carried at Re = 50,000-450,000 (Stein and Murray 2005; Johari *et al*. 2007; Miklosovic *et al*. 2004; Hansen *et al*. 2011; Skillen *et al*. 2015; Cai *et al*. 2017; Custodio 2007; Cai *et al*. 2015). Separation delay and increased maximum stall angle (Watts and Fish 2001; Miklosovic *et al*. 2004; Carreira Pedro and Kobayashi 2008) and reduced drag (Miklosovic *et al*. 2004; Hansen *et al*. 2011; Rostamzadeh *et al*. 2013) are also reported. These investigations mostly considered thick airfoils at different Re; NACA0020 airfoil at Re = 250,000, for 0deg ≤ *AOA* ≤ 12deg by Stein and Murray (2005), NACA63-021 airfoils by Johari *et al*. (2007) at Re = 183,000 at pre-stall, experiments by Hansen *et al*. (2016) at Re = 120,000 using NACA0021 and 65-021 airfoils, NACA63-021 airfoils at Re = 50,000 over a range of AOAs from 0deg to 90deg by Zhang and Frendi (2016), NACA0018 airfoil by Arai *et al*. (2010) at Re = 138,000, NACA0030 airfoil at *Re* < 100,000 by Bolzon *et al*. (2016), NACA0030 airfoil at Re between 50,000 and 290,000 by de Paula *et al*. (2017), NACA0012 airfoil Serson *et al*. (2017) at Re = 10,000 and 50,000, NACA63-021 by Cai *et al*. (2017).

In the second type of study, the effect of tubercles on the performance of three dimensional wing models was investigated (Miklosovic *et al*. 2004; Miklosovic *et al*. 2007; Stanway 2008; Bolzon *et al*. 2016; Bolzon *et al*. 2017a; Bolzon *et al*. 2017b; Wei *et al*. 2018). The results obtained differed depending on the wing planform geometry, aspect ratio, taper ratio, Re and sweep angle.

Several theories put forward to explain the flow mechanism were responsible for the improvement in the performance of the tubercled airfoil. The main mechanisms include the vortex generator analogy (Miklosovic *et al*. 2004; Zhang and Frendi 2016), boundary layer momentum exchange and flow compartmentalization Watts and Fish (2001), a functional similarity to small delta wings (Custodio 2007; Stanway 2008; Wei *et al*. 2015), and low pressure at troughs and variation of effective AOA (Van Nierop *et al*. 2008; Weber *et al*. 2011; Bolzon *et al*. 2017b), inhibition of the spanwise progression of stall (Johari *et al*. 2007), Hansen *et al*. (2011) and Custodio (2007), Varying Spanwise Circulation (Rostamzadeh *et al*. 2013; Rostamzadeh *et al*. 2014; Cai *et al*. 2015; Bolzon *et al*. 2017a), Formation of a Vorticity Canopy (Hansen *et al*. 2016) Weakening of the Suction Peak (Serson and Meneghini 2015), the formation of streamwise vortices caused by a Kelvin-Helmholtz instability (Favier *et al*. 2012).

Numerical simulations are cost-effective tools to understand better the complex flow physics associated with the tubercled airfoil. Experimental results were successfully validated, and flow features were accurately predicted by various computational methods, including the potential flow theory (Panel Method), Reynolds Averaged NavierStokes (RANS), Large Eddy Simulation (LES), Detached Eddy Simulation, direct numerical simulations (DNS) (Van Nierop *et al*. 2008; Carreira Pedro and Kobayashi 2008; Ozen and Rockwell 2010; Serson *et al*. 2017; Filho *et al*. 2018)

The low computational cost and reliability make the RANS methods the most convenient tool for CFD simulation to analyse the complicated flow phenomena. Nevertheless, accurate prediction of boundary layer transition and modelling of the LSB is difficult with the frequently used RANS models such as k–ω, k–ε (Crivellini *et al*. 2014). The LES and DNS are the turbulence models that can reliably predict the LSB, but the computational cost is high (Sheikholeslami and Domiri Ganji 2017). The transition model proposed by (Menter *et al*. 2006a) is based on γ and can be combined with available CFD codes. The noticeable advantage of this model is that the experimental data can be associated with transition modeling (Shah *et al*. 2015). The model is popular because of its ability to predict flow transition phenomena at a low computational cost. Lu *et al*. (2021) studied the performance of optimized tubercled airfoil using the RANS transition model and validated it with experimental results. The effect of tubercles on the performance and the related flow structure on a ducted propeller for marine application were investigated by Stark *et al*. (2021) using the RANS transition model. Similarly, many researchers have used the model to model the transition flow (Cai *et al*. 2017; Rostamzadeh *et al*. 2013; Hansen *et al*. 2016).

The detailed literature presented above indicates that there is no consistency in the results obtained regarding the effects of tubercles on the aerodynamic performance and no consensus on the mechanism responsible. Further, the effect is airfoil specific, depends on Re and AOA. In the present work, a numerical investigation is carried with γ–Re_θ transition model for understanding the effect of tubercles on the performance of a low Re airfoil. The E216 airfoil is considered for the study. It exhibits good aerodynamic performance at low Re, making it a good candidate for SSWT blades (Sreejith and Sathyabhama 2018). The simulations are carried at Re of 100,000 which is representative of SSWT operational condition. Formation of LSB is expected at such low Re. Hence, the particular interest of the present investigation is to explore the effect of the sinusoidal leading edge on the LSB and the flow structure. Another primary interest is to obtain information on the effect of amplitude and wavelength of tubercle. Literature data (Sreejith and Sathyabhama 2018) is used as a benchmark for validating the simulation method.

Fig. 1. Tubercles on humpback whale flippers (Hansen 2012).

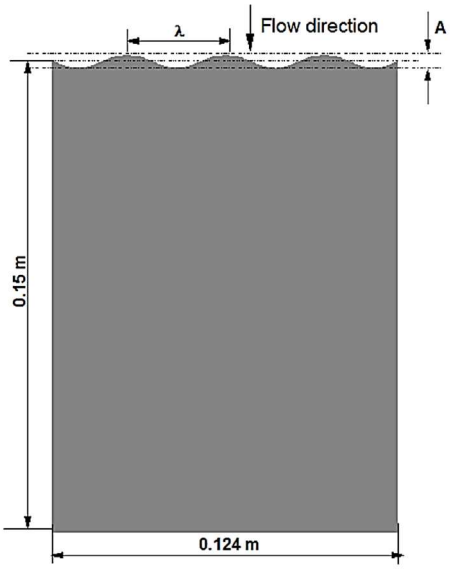

Fig. 2. Tubercle model showing the dimensions and nomenclature.

2. NUMERICAL METHODOLOGY

2.1. Geometry

The airfoil employed as a geometry cross-section for both baseline and tubercle models in the present work is E216. SolidWorks 2010 is used for airfoil geometry creation. The plain model has a chord length of 150 mm and for the tubercle models, an average chord length of 150 mm is maintained. A total of nine tubercle configurations, formed by different combinations of amplitude and wavelength, are studied in the present work. The nomenclature of the model is given in Fig. 2, where A represents amplitude and W represents wavelength in mm. The model names are given as 'A(x)W(y)' where 'x' and 'y' represent the corresponding amplitude and wavelength in mm. The values used here for amplitude and wavelength are based on the data of an actual whale flipper (Fish and Battle 1995). The average amplitude and wavelength of the whale flipper normalised with its average chord length are 0.05 and 0.41, respectively. The corresponding values of amplitude and wavelength are approximately 8 mm and 62 mm. As far as a SSWT blade is concerned, going for higher amplitude and wavelength than the calculated one may invite structural challenges. So, the study is carried out with two lesser amplitude and wavelength values. The details of the tubercled models studied in the present work are given in Table 1.

Table 1. Tubercle model parameters

		Wavelength(mm)		
		15.5	31	62
Amplitude(mm)	2	A2W15.5	A2W31	A2W62
	4	A4W15.5	A4W31	A4W62
	8	A8W15.5	A8W31	A8W62

2.2 Computational domain and mesh

A three dimensional computational domain of rectangular shape is used for simulation and the domain (Fig. 3) and meshes (Fig. 4) are created using ICEM CFD of ANSYS 15.0 similar to that we used in our previous paper (Sreejith and Sathyabhama 2020). The total length of the computational domain is set to 25 times the chord length(c): 9c in front of the airfoil and 15c behind the airfoil to achieve fully developed flow. The width is 20 times the chord length. The resolution of the mesh is higher in the region close to the airfoil, where greater

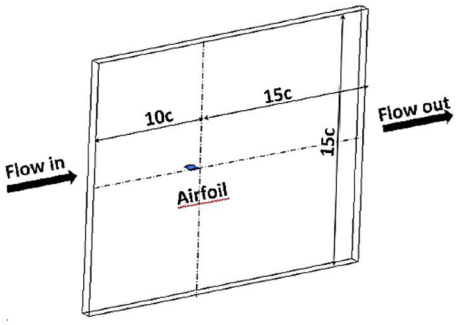

Fig. 3. Computational domain (Sreejith and Sathyabhama 2020).

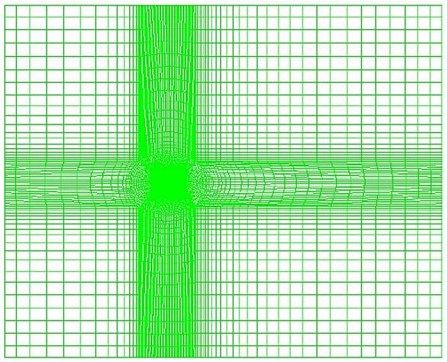

Fig. 4. Far view of structured grid in the domain (Sreejith and Sathyabhama 2020).

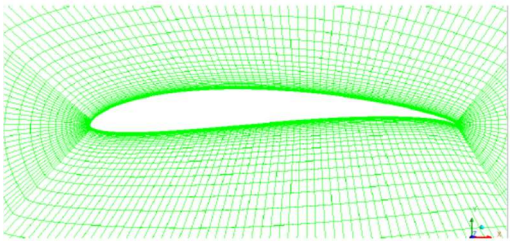

Fig. 5. Close view of dense grid nearer to the airfoil (Sreejith and Sathyabhama 2020).

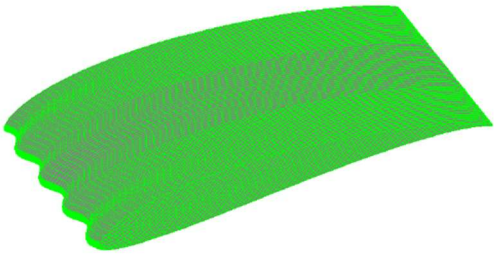

Fig. 6. Grid on the airfoil surface (Sreejith and Sathyabhama 2020)

computational accuracy is needed, as shown in Figs. 5 and 6. As per the requirements of the Turbulent models used, the height of the first cell adjacent to the surface is set in such a way that it results in y^+ value less than one.

No-slip boundary condition is imposed on the airfoil, whereas velocity inlet at flow inlet, wall boundary condition at top and bottom boundaries, symmetry condition at sidewalls and pressure outlet at the outlet of the domain are used. The fluid properties are calculated for a free stream temperature of 308 K, same as the environmental temperature in which the baseline experiments were carried out. For Re of 100,000, and airfoil chord length of 150 mm, free stream inlet velocity of air is calculated to be 10.08 m/s. Flow is considered as incompressible. To solve momentum equations semi-implicit method for pressure linked equations (SIMPLE) algorithm (FLUENT 2014) and second order upwind spacial discretization is employed in the calculations. The least square cell-based method is set for spatial gradient. Residual target value of 10^{-6} is set as convergence criteria.

2.3 Turbulence model

Langtry-Menter 4-equation Transitional SST Model or $\gamma-Re_\theta$ - SST model is used in the study (Menter *et al.* 2006b). It is well-proven for transition prediction in many test cases including flow over airfoil (Chishty *et al.* 2011). Hence, the same model is used in the present work. The model is based on the two-equation $k-\omega$ SST model, augmented by two additional equations, one for intermittency (γ) and another for transitional Reynolds number ($Re_{\theta t}$) to describe the laminar-turbulent transition process. Intermittency term is employed to activate the production term of the turbulent kinetic energy (TKE), downstream of the transition point in the boundary layer, and the Transition Reynolds number term captures the non-local effect of the turbulence intensity (Menter *et al.* 2006b). The governing equations involved in this analysis are listed below (FLUENT 2014).

The transport equation for the intermittency term γ is given in Eq. 1.

$$\frac{\partial(\rho\gamma)}{\partial t}+\frac{\partial(\rho U_j\gamma)}{\partial x_j}=P_{\gamma1}-E_{\gamma1}+P_{\gamma2}-E_{\gamma2}+\frac{\partial}{\partial x_j}\left(\mu+\frac{\mu_t}{\sigma_\gamma}\right)\frac{\partial\gamma}{\partial x_j} \tag{1}$$

where, $P_{\gamma1}$, and $E\gamma1$ are the transition source terms. The value of constants used in the intermittency equations are, $c_{\gamma1}=0.06$; $c_{e2}=50$; $c_{\gamma3}=0.5$ and $\sigma_\gamma=1.0$.

Equation for transition momentum thickness number, $R\tilde{e}_{\theta t}$, is given by Eq. 2.

$$\frac{\partial(\rho R\tilde{e}_{\theta t})}{\partial t}+\frac{\partial(\rho U_j R\tilde{e}_{\theta t})}{\partial x_j}=P_{\theta t}+\frac{\partial}{\partial x_j}\left[\sigma_{\theta t}(\mu+\mu_t)\frac{\partial R\tilde{e}_{\theta t}}{\partial x_j}\right] \tag{2}$$

where $P_{\theta t}$ is the blending function used to turn off the source term in the boundary layer.

Values of the constants in the Eq. 2 are, $c_{\theta t}=0.03$ and $\sigma_{\theta t}=2.0$. Previous research by Fagbenro *et al.* (2014) and Shah *et al.* (2015) proved that more realistic results are obtained with the turbulence model when the coefficient values for $c_{\theta t}$ and $\sigma_{\theta t}$ 0.02 and 3.0 respectively. In the present work the same values for the coefficients are used.

Separation - induced transition correction

Separation-induced transition can be re written as (Menter *et al.* 2006a),

$$\gamma_{sep}=min\left[2.max\left[\left(\frac{Re_v}{3.235Re_{\theta c}}\right)-1,0\right]F_{reattach},2\right]F_{\theta t} \tag{3}$$

where

$$F_{reattch}=e^{-\left(\frac{R_T}{20}\right)^4} \tag{4}$$

$$\gamma_{eff}=\max(\gamma,\gamma_{sep}) \tag{5}$$

Coupling the Transition Model with SST Transport Equations

The transition model interacts with the SST turbulence model with modification in the k-equation as below (Menter *et al.* 2006a):

$$\frac{\partial(\rho k)}{\partial t}+\frac{\partial(\rho u_i k)}{\partial x_i} = \frac{\partial}{\partial x_i}\left(\Gamma_k \frac{\partial k}{\partial x_j}\right)+G_k^*-Y_k^*+S_k \quad (6)$$

where,

$$Y_k^* = \min(\max(\gamma_{eff},0.1),1.0)Y_k \quad (7)$$

and

$$G_k^* = \gamma_{eff} G_k \quad (8)$$

where Y_k and G_k are the terms representing original destruction and production respectively for the SST model. The production term in the ω-equation is used without any modification.

Five different meshes are prepared for gridindependent study with number of grid cells ranging from 700,362 to 2,141,000. Simulations are carried out for AOA of 6° and the results are shown in Fig. 7. After around 1,237,620 grid cells there is no significant variation in lift coefficient and hence it is considered as appropriate mesh size for further simulations.

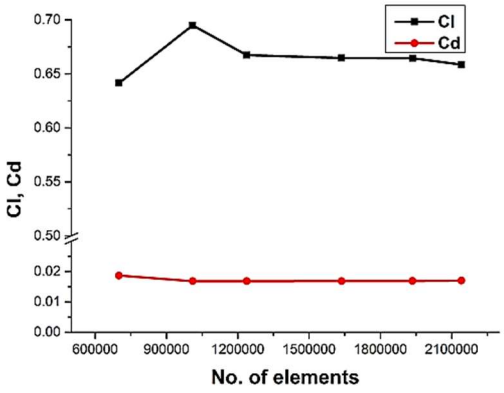

Fig. 7. Variation of C_l and C_d of the airfoil for different grid number at AOA of 6°.

3. RESULTS AND DISCUSSION

3.1 Validation of numerical simulation

The results obtained from simulation are validated with the experimental results reported in our previous work (Sreejith and Sathyabhama 2018). The C_l and C_d values obtained from the experiments and the simulations are plotted against the AOA in Fig. 8. There is an acceptable level of agreement between simulation and experimental results. However, the limitation of the RANS model to accurately predict the boundary layer separation and the transition is evident from the Fig. 8 as the numerical results deviate from the experimental results in the stall region (Rahimi *et al*. 2014). The simulation underpredicts the lift coefficient up to AOA of 8°, and after that, it overpredicts, the mean difference being 5.81%. The drag coefficient is

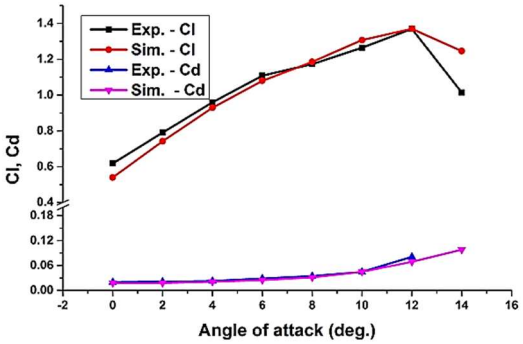

Fig. 8. C_l and C_d results obtained from experiment and simulation as a function of AOA (Sreejith and Sathyabhama 2018).

underpredicted in the range of the AOA studied in this work by 4.31%. The combination of various numerical schemes with turbulence models and grid density may be the reasons for the deviation of the results. Pure air properties are used for simulation (without moisture and salt contents), whereas in experiment air may contain impurities, this could be another reason for the mismatch in the results. This investigation aims to study the effect of tubercles in the pre stall region, where the difference in results is small enough.

The computational result (Fig. 8) depicts a linear variation of C_l up to an AOA of 12° at which the maximum C_l is 1.37. The region after the AOA of 12° represents the flow transition or stall. In the experimental approach, wake surveys have been conducted up to stall AOA, and drag coefficients are calculated. Beyond the stall AOA, the wakes will be too large to survey. Hence, the C_d results are presented up to stall AOA only. At stall, C_d of 0.069 is obtained, and a drastic increment is observed thereafter.

A comparison of the results obtained from the experiments and generated from CFD for the C_l/C_d ratio is presented in Fig. 9. The maximum values are 44.39 and 42.47, respectively, in simulation and experiment at AOA of 4°. The measured results deviate from the simulation results by 8.21%.

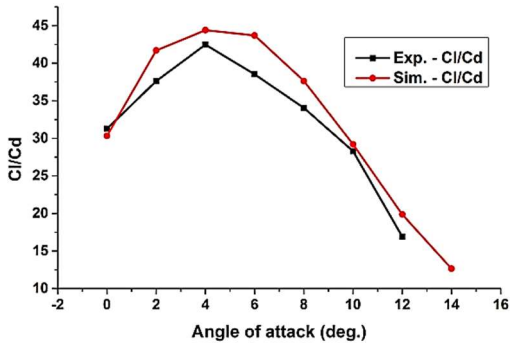

Fig. 9. C_l /C_d results obtained from simulation along with experimental results as a function of AOA

3.2 Effect of leading edge tubercles on aerodynamic performance of the airfoil

The influence of tubercles on the aerodynamic characteristics (lift, drag, and lift to drag ratio) of E216 airfoil at Reynolds number of 1,00,000 is discussed in this section.

The effects of tubercle parameters on the performance of the airfoil is depicted in Figs. 10a - 10c. Figure 10a shows the effect of varying amplitude from 2 mm to 8 mm at a constant wavelength of 62 mm on the performance of the airfoil. The trend in the variation of C_l with AOA is similar for all the tubercled models and the baseline till AOA ≈ 10°. The baseline airfoil stalls at AOA of 12°. The models A2W62 and A8W62 have slightly better performance compared to the baseline. The advantage is minimal at lower AOA (≤ 4°) and better at higher AOA (4° ≥α≤ 10°). Both the models stall at AOA of 10°. The plain model has a higher C_l value (1.31) at AOA of 10° compared to the other two models. The most significant improvement of 5.14% in C_l is obtained for A2W62 at AOA ≈ 8°.The model A4W62 produces lower Cl than all other models, as shown in Fig. 10a. Unlike other airfoils, A4W62 stalls at AOA ≈ 12° and generates the highest C_l of 1.33 among the group.

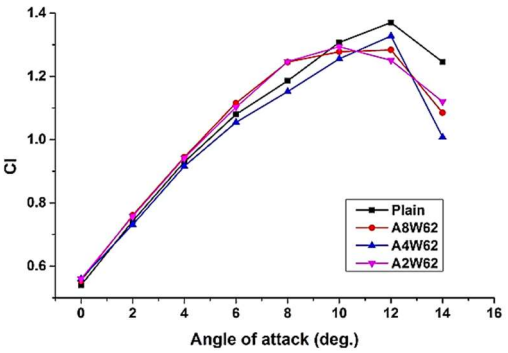

(a)

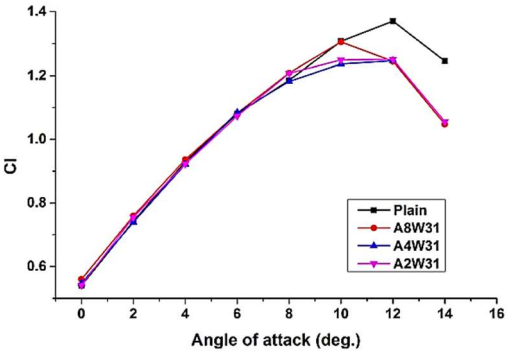

(b)

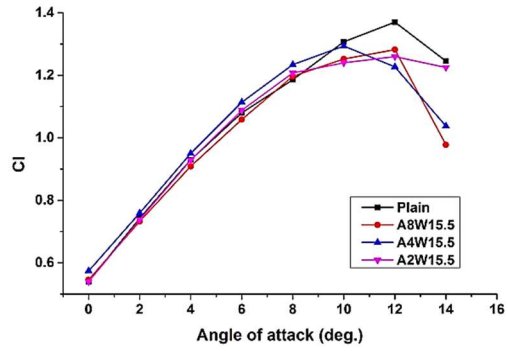

(c)

Fig. 10. Effect of amplitude on C_l of airfoil.

When the wavelength is 31 mm, no significant variation in C_l values is observed and the trend is same for the tubercled and the baseline models till AOA ≈ 8° as shown in Fig. 10b. The model with the highest amplitude (A8W31) stalls at AOA ≈ 10° and generated C_l roughly equal to that for the baseline. The other two airfoils configurations stall at AOA≈ 12° and have smooth C_l variations from 10° to 12 and produce lower C_{lmax} than baseline airfoil.

For airfoil models with wavelength 15.5 mm, C_l variation with respect to AOA followed the same trend as the baseline till AOA ≈ 10° as shown in Fig. 10c. Model A4W15.5 generates a higher lift than other models till stall angle. The model stalls at lower AOA (10°) compared to the baseline. A maximum lift improvement of 4.1% is observed at 8° AOA. The stall angle increased from 10° to 12°. The model A2W15.5 exhibits comparatively smooth Cl variation, particularly after 8° AOA.

The major observations lead to the fact that mainly two parameters attribute smooth C_l characteristics: amplitude and amplitude to wavelength ratio. Among the studied tubercled models, those with the least amplitude (2mm) exhibited smooth C_l characteristics, especially near the stall angle, which is similar to the observation of Hansen (2012) and Sudhakar *et al.* (2019). Models with amplitude to wavelength ratio of 0.13 (A2W15.5, A4W31 and A8W62) exhibit similar characteristics. Apparently, prestall C_l improvement is observed for the models with an amplitude to wavelength ratio of 0.26 only, which matches with the observation of Favier *et al.* (2012).

Figure 11 shows the effect of varying amplitude on C_d generated by the airfoils. Similar to the findings of Cai *et al.* (2017), the C_d produced by all the modified airfoils are higher than the unmodified one. No clear benefit can be observed by providing tubercles at the leading edge. The drag produced by all the models is almost same in the lower AOA range (α ≤ 6°) and the deviation increases with an increase in AOA. A highest C_d is observed for the A2W15.5 configuration. The same trend is observed when the wavelength is varied.

Figures 12 represent the combined effect of C_l and C_d and the ratio predicts whether the modification is beneficial or not. The plain model has a maximum C_l/C_d ratio of 44.39 at ≈ 4°. Except for A2W62, all other tubercled models follow the same trend as that of unmodified one. All tubercled models have maximum C_l/C_d at AOA ≈ 4° except for A2W62, which has the maximum ratio at AOA = 6°. Except for A2W62 and A8W31, no other models show better performance than the unmodified one.

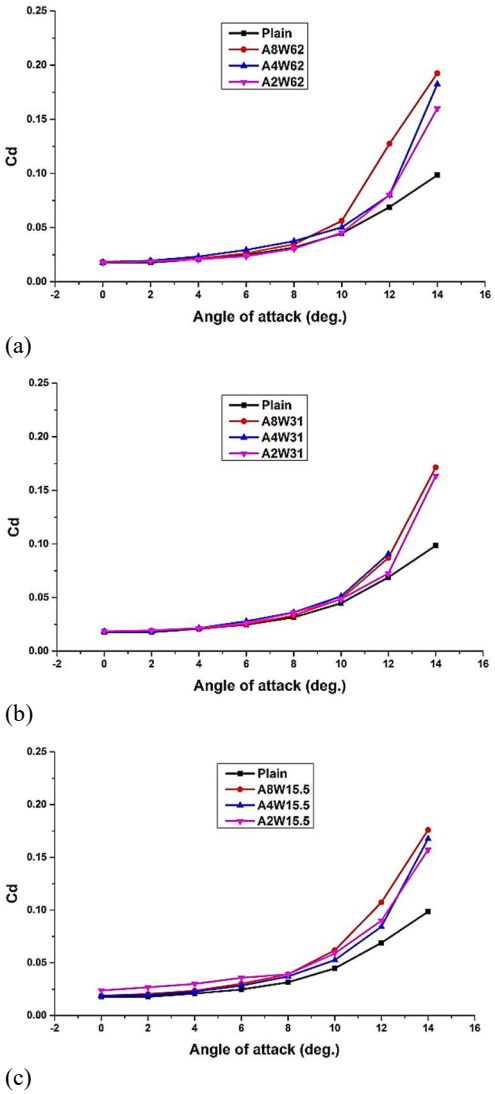

Fig. 11. Effect of amplitude on C_d of airfoil.

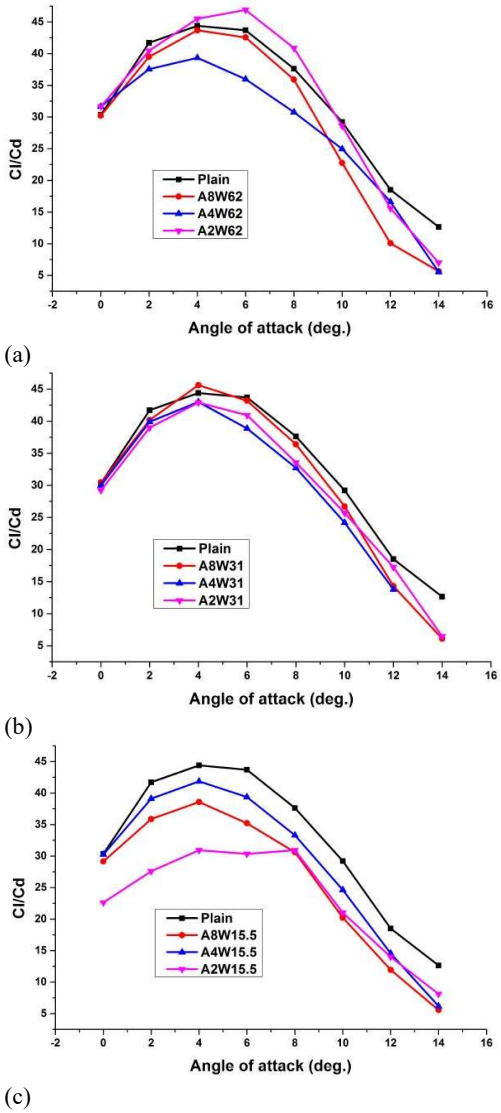

Fig. 12. Effect of amplitude on C_l/ C_d of airfoil.

Wei *et al*. (2018) also reported similar observation on swept back wing. The model A8W31 generated a 2.78% higher C_l/C_d ratio than the unmodified one at AOA of 4°. The highest C_l/C_d ratio of 46.91 at AOA of 6° is observed for A2W62. The value is 7.37% higher at AOA of 6° and 5.68% higher at AOA of 4° compared to the unmodified model.

3.3 Surface pressure

Figures 13-15 shows the surface pressure coefficient (C_p) distribution against x/c location along the stream-wise direction on tubercled and baseline models at an AOA of 4°. The C_p distribution on the plain model is plotted at midspan and for the tubercled models at two span-wise locations, one passing through the crest and the other through the trough. The suction peak of -1.05 is observed for the plain model at the the upper surface leading edge (Fig. 13a) and the flow accelerates thereafter. A clear pressure plateau is observed on the suction surface. The pressure plateau is an indication of the LSB formation (Hu and Yang 2008). The boundary layer separates at a distance of x/c = 0.48, the beginning of pressure plateau in the C_p plot, with subsequent reattachment at x/c = 0.79 from leading-edge for the plain model. As shown in the figure, the length of LSB is observed to be around 0.31c for the plain model.

Figures 13a - 13c show the C_p distribution on tubercled models with varying wavelengths and for a constant amplitude of 2 mm, along with that for the unmodified model. At leading-edge, the tubercled models have slightly higher C_p along the peak and lower along the trough on the upper surface compared to the baseline. But for the model with lowest amplitude and wavelength (A2W15.5), No significant change in the magnitude and location of the suction peak have been observed at the tubercle peak region (Fig. 13a). However, an increase in peak suction pressure (-1.18) is observed for the trough region of the tubercle. A vague pressure plateau is formed close to trailing edge, represents a very weak LSB, for both peak and trough regions of the tubercle. The boundary layer leaves the airfoil surface at 0.63c and reattaches at 0.92c, forming an LSB of size 0.29c. The bubble is shortened by 6.5%,

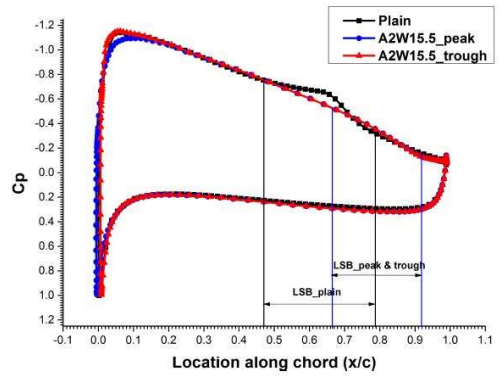

(a)

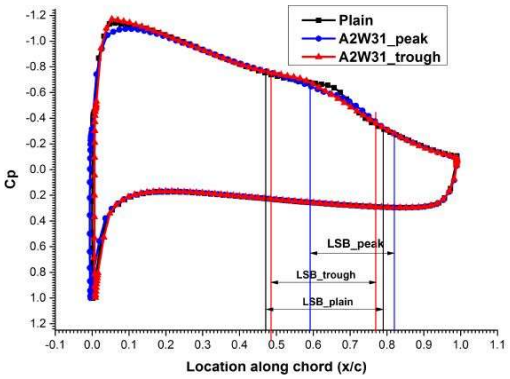

(b)

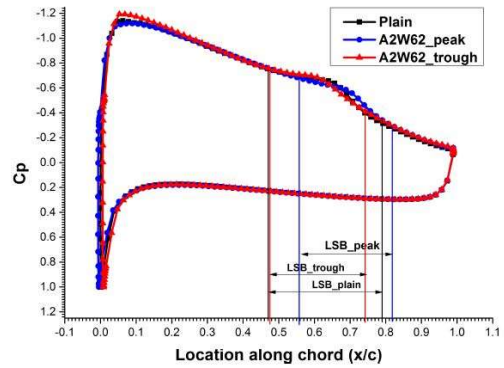

(c)

Fig. 13. C_p distribution on plain and tubercled models at AOA of 4°; (a) A2W15.5, (b) A2W31 and (c) A2W62.

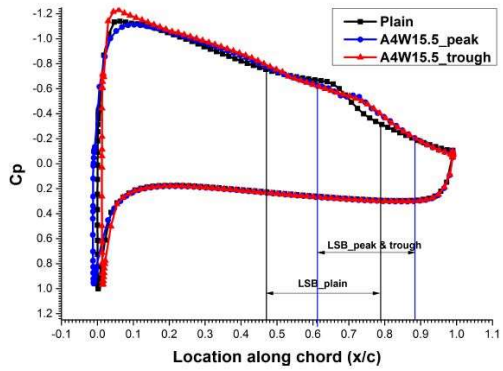

(a)

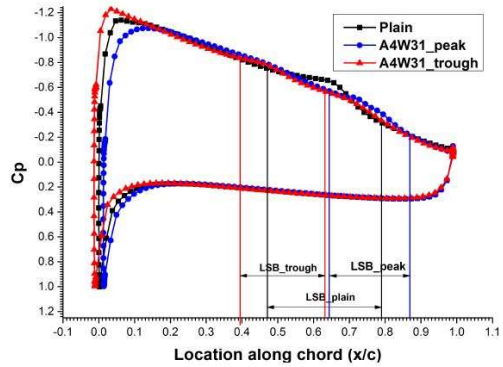

(b)

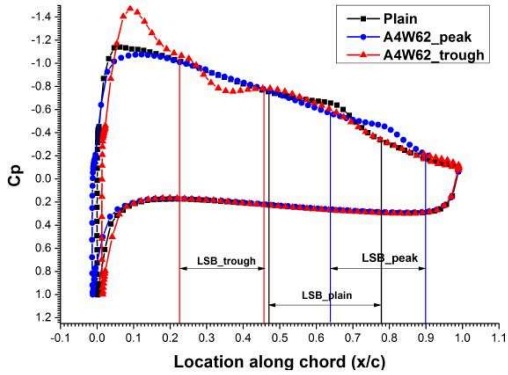

(c)

Fig. 14. C_p distribution on plain and tubercled models at AOA of 4°; (a) A4W15.5, (b) A4W31 and (c) A4W62.

relative to that on the plain airfoil. The Peak and trough sections of the tubercle record a maximum suction pressure values of -1.08 and -1.24, respectively, in the case of A4W31, as evident in Fig. 14b. The corresponding value for the plain airfoil lies in between these two values. Notably, the LSB is more robust than that formed on A2W15.5. The surface pressure coefficient distribution plots suggest that the flow on the trough and peak regions undergo separation and reattachment at different chordwise positions compared to the plain airfoil. This gives rise to a spanwise wavy LSB for the tubercled airfoil, as opposed to the straight LSB on the plain airfoil. The relatively low chordwise pressure gradients between $0.39 \leq x/c \leq 0.63$ indicate that the LSB of length 0.24c is formed behind the trough. The corresponding low-pressure region for the tubercle peak lies between$0.65 \leq x/c \leq 0.87$, resulting in LSB of length 0.22c. The percentage reduction in the length of the bubble is 25.8% when compared with that of the plain airfoil.

Figure 15c shows that the magnitude of the suction peak is -1.04 and -1.38, respectively, for the tubercle peak and trough sections, in the case of A8W62. The flow separates at a distance of 0.37 and 0.65 respectively from the leading edge and subsequently reattaches at x/c = 0.58 and 0.90 behind the trough and peak regions. This results in an LSB length of 0.21c, and 0.25c respectively, for the trough and peak regions of the tubercle and 25.8% reduction in length. The wavy LSB is not very intense, as in the case of the plain airfoil. It is noteworthy that, pressure coefficient distribution on the lower surface of the airfoil with and without tubercles considered

Table 2. Laminar separation bubble location and size on baseline and tubercled models

Model	Laminar Separation bubble					
	Trough			Peak		
	Begin(x/c =)	End(x/c =)	Length(%c)	Begin(x/c =)	End(x/c =)	Length(%c)
Plain	0.48	0.79	0.31	0.48	0.79	0.31
A2W15.5	0.63	0.92	0.29	0.63	0.92	0.29
A2W31	0.49	0.77	0.28	0.59	0.82	0.23
A2W62	0.48	0.74	0.26	0.55	0.81	0.26
A4W15.5	0.61	0.88	0.27	0.61	0.88	0.27
A4W31	0.39	0.63	0.24	0.65	0.87	0.22
A4W62	0.23	0.46	0.23	0.64	0.90	0.26
AW15.5	0.65	0.87	0.22	0.65	0.87	0.22
A8W31	0.38	0.60	0.22	0.69	0.90	0.21
A8W62	0.37	0.58	0.21	0.65	0.90	0.25

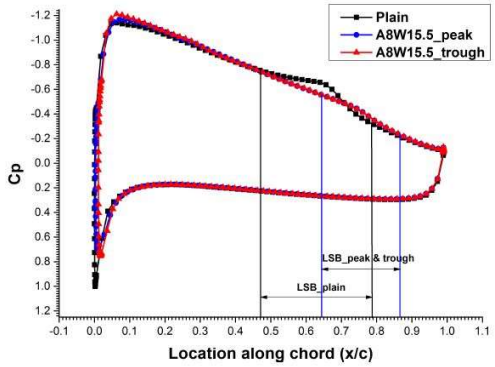

(a)

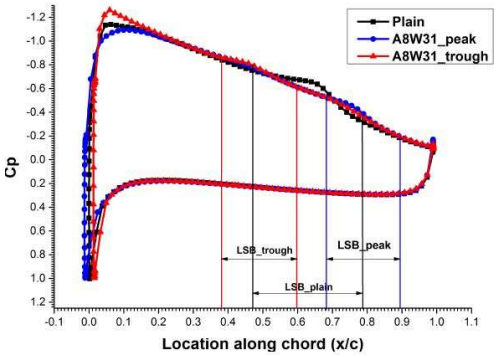

(b)

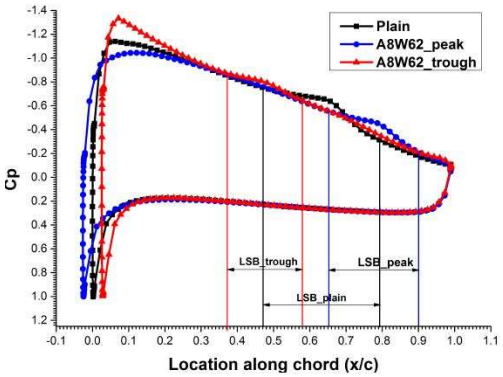

(c)

Fig. 15. C_p distribution on plain and tubercled models at AOA of 4˚; (a) A8W15.5, (b) A8W31 and (c) A8W62.

above, follow the same trend. The preceding results are in coherence with the observations of Sudhakar *et al*. (2019), Skillen *et al*. (2015) and Serson *et al*. (2017). The details regarding the flow separation point, reattachment point, and bubble size for all the models are listed in Table 2.

3.4 Surface flow pattern analysis

Figure 16 shows the surface streamlines on the suction surface of the baseline airfoil at AOA of 4˚. The region of LSB is clearly visible in the surface streamline pattern and is in-line with the C_p distribution. The flow separates at nearly 0.47c represented by the reduced density of streamlines. A clear parting line can be observed at the reattachment point (R). Thereafter the flow continues as turbulent. Such surface features are in agreement with the literature data (Sudhakar *et al*. 2019).

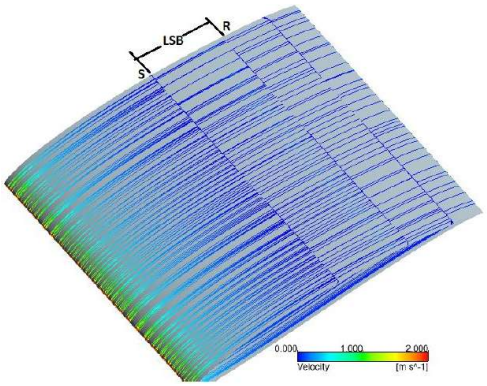

Fig. 16. Surface streamline pattern on plain airfoil model at AOA of 4˚.

The flow structure over the modified airfoils at AOA 4˚ is shown in Figs. 17-19 for various combination of amplitude and wavelength. The model with the least amplitude and wavelength (A2W15.5) (Fig. 17a) shows no sign of the LSB as observed in C_p plot. Tubercle completely eliminated the LSB and stream-lines are attached over the entire surface of the airfoil. Increase in wavelength to 31mm results in a complex flow pattern over the surface compared as shown in Fig. 17b, similar to the preceding observation of Rostamzadeh *et al*. (2014). A certain portion of the flow emerging from leading edge moves from peak to trough and interacts with the incoming flow in the trough and forms a recirculation region (primary counter rotating vortex pair (CRVP)) in the trough. Once the flow achieved

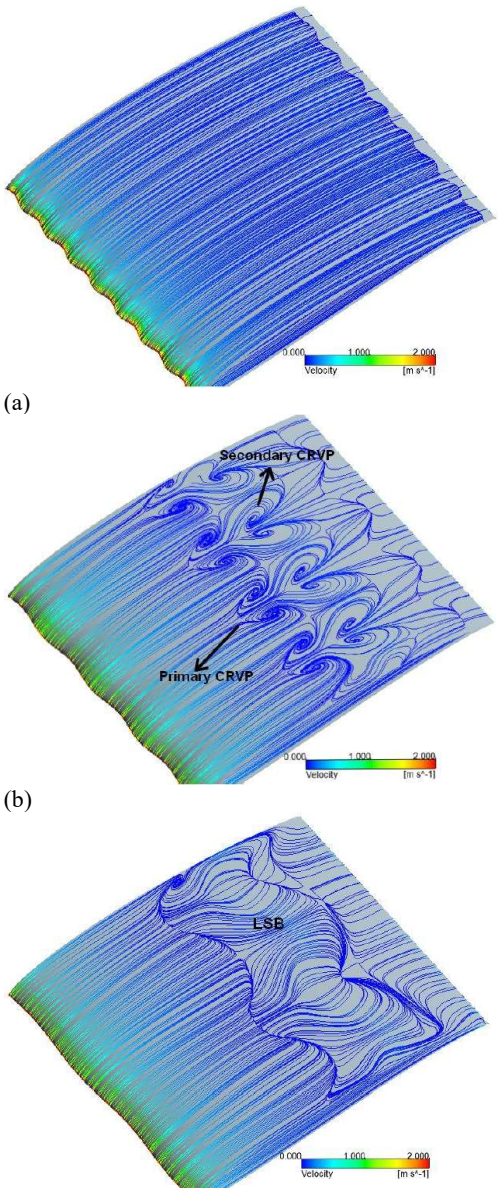

Fig. 17. Streamlines distribution over modified airfoils; (a) A2W15.5, (b) A2W31 and (c) A2W62.

enough energy, the total flow is divided into two parts- one part which moves straight towards the trailing edge and the other part moves from trough to peak along with its stream-wise motion. After traveling downstream, the straight flow continues as it is, whereas the other part of the flow moves again to the trough and forms secondary CRVP. The LSB is formed on the model as observed in C_p distribution curve and its position along the peak and trough are at different stream-wise locations. The point where the primary vortex forms serves as the starting point of LSB in trough, whereas the formation of secondary vortex is the starting point of LSB along the peak. Since the secondary vortices are formed downstream of the primary vortices, the flow separation along the trough is ahead of that along the peak. As a result, the LSB forms in a sinusoidal manner.

When the wavelength is increased to 62 mm (A2W62) (Fig. 17c) there is no clear spot of span-wise primary vortex formation, instead, a smooth attached flow is exhibited. The flow gets gradually redirected from the peak to the trough over the distance up to mid-chord length from leading edge, then starts flow separation pertaining to the formation of the LSB. The flow gets reenergized while it propagates towards the trailing edge due to turbulent mixing from the span-wise flow and finally forms an attached turbulent flow near to trailing edge. A clear parting line for flow separation and reattachment can be observed in a sinusoidal manner along the span-wise direction. The location of LSB along trough is ahead of that at peak in stream-wise direction. The higher wavelength and lower amplitude of tubercle attribute to gradual surface texture change. This resulted in low pressure gradient between the trough and peak region. As a result, the initial span wise flow is less dominating and hence the primary vortex are absent in this situation. It substantiates the relation between tubercle wavelength and number of vortex formation. The larger the wavelength, lesser will be the counter rotating vortex formation (Wei *et* 2019)

Multiple small vortices are formed along the stream-wise direction on the model with a medium amplitude of 4 mm and least wavelength of 15.5 mm (A4W15.5) as depicted in Fig. 18a which again evince the strong relationship between wavelength of tubercles and the vortex formation as narrated in the previous section. Two kinds of primary vortex formation are observed on the trough of the airfoil surface. A stronger vortex formation, which is tri-periodic with comparatively weaker vortices in the two troughs in between, is observed. Both types of vortices start from the same location along the span-wise direction which represents the beginning of laminar separation. The observations closely match with that reported by Wei *et al*. (2019). After the formation of multiples vortices, finally, the flow reattaches near the trailing edge. Also, the LSB formation occurs at the same chord-wise location along the peak and trough, and the same is depicted in the C_p plot discussed in the previous section.

When the wavelength is increased to 31 mm (A4W31) (Fig. 18b) the streamline pattern formed is exactly similar to that for the A2W31 but differs only in size. Since the amplitude is increased, more shallow flow passages are formed which results in elongated vortices of smaller span-wise size. The laminar separation points are represented by the beginning of vortices as described earlier. But the tubercled airfoil A4W64 (Fig. 18c) does not shows any clear symmetric vortices. The significant cross flow in span-wise direction due to high wavelength lead to well mixing of fluid is the reason for this flow characteristics.

Further increase in amplitude to 8 mm with a wavelength of 15.5 mm (A8W15.5) makes the surface with deep bumps. This restricts the flow along the stream-wise direction and slightly energized flow delays the LSB formation or vortex formation. The counter-rotating vortices are formed

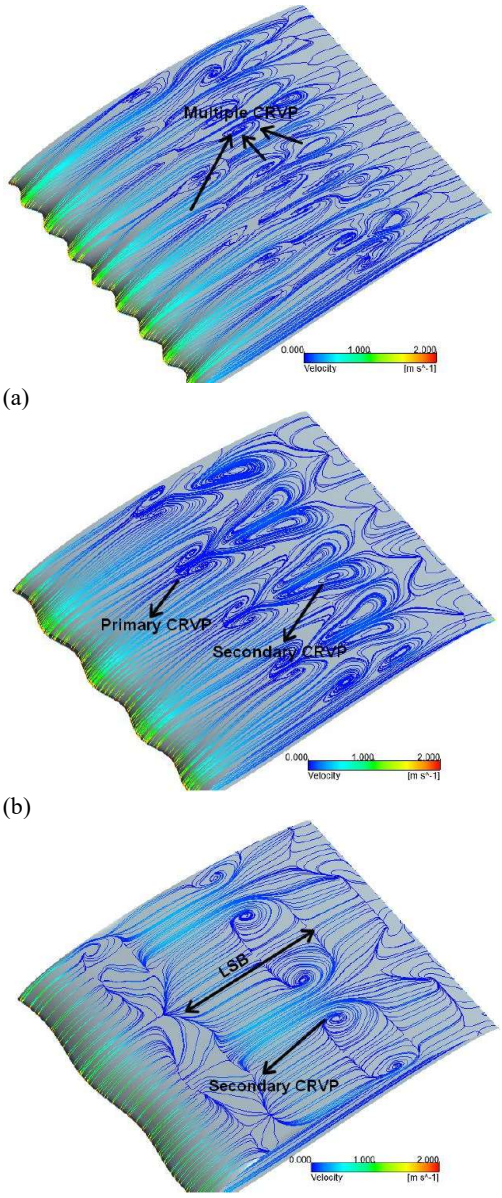

(a)

(b)

(c)

Fig. 18. Streamlines distribution over modified airfoils; (a) A4W15.5, (b) A4W31 and (c) A4W62.

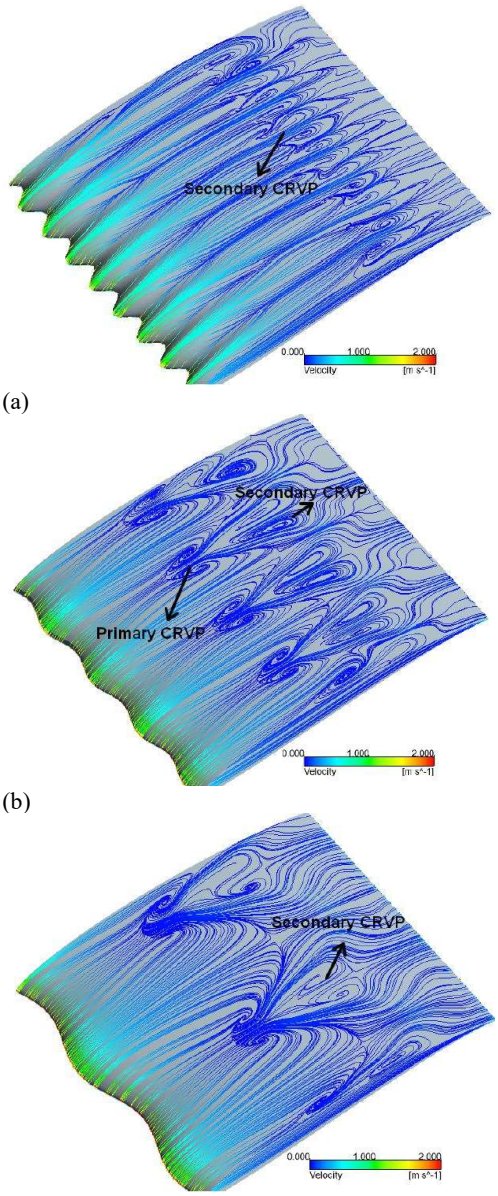

(a)

(b)

(c)

Fig. 19. Streamlines distribution over modified airfoils; (a)A8W15.5, (b)A8W31 and (c)A8W62.

in the region between peak and trough at the same chord-wise location along the span Fig. 19a.

As the wavelength increase to 31mm (A8W31, Fig. 19b) and 62 mm (A8W62, Fig. 19c), vortex formation is same as in the respective models with amplitude 2 mm and 4 mm as described previously with the slight difference only in the strength and shape of vortices. As the amplitude is increased, the vortices become longer in the chord-wise direction and shorter in width. Further, the primary vortices become more dominant with an increase in amplitude.

The modified airfoil models generate lift equal to that produced by the plain model. This trend is similar to that for vortex generator (Stein and Murray 2005) and hence the pair of counter-rotating vortices act like vortex generator. The presence of stream-wise, counter-rotating vortices will thin the boundary layer in down-wash areas on the airfoil surface (Bolzon *et al*. 2015).This results in increased near-wall velocity gradient, which results in increased shear stress. This increased shear stress induces additional skin friction drag and net increase in total drag of the tubercled models as seen in Fig.11. It is seen that as the spacing between the tubercles is reduced (cases with wavelength 15.5 mm) they act more like a turbulence generator and there is more uniform boundary layer mixing and attachment of boundary layer over the airfoil surface. This mixing makes the flow turbulent and produces detrimental effect on the performance as it was found for vortex generator (Godard and Stanislas 2006). This is the reason for the reduced performance of model with the least wavelength (15.5 mm) even with the LSB elimination.

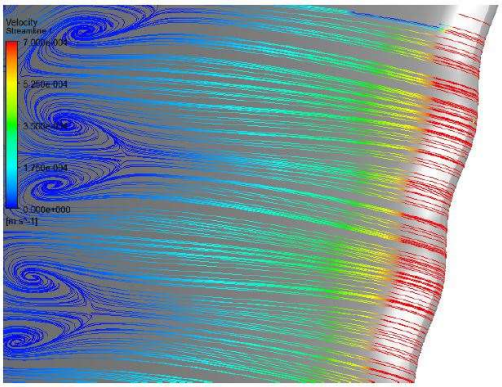

Fig. 20. Velocity stream lines on A2W31 at AOA of 4◦, showing velocity variation at different stream-wise and span-wise locations.

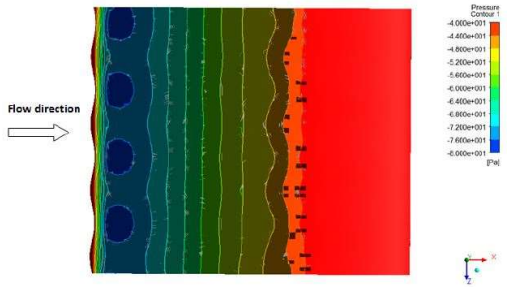

Fig. 21. Pressure contour on A2W31 at AOA of 4°, showing pressure variation at peak and trough.

Figure 20 shows the velocity variation at different stream-wise and span-wise locations on A2W31 model at AOA of 4°. It can be seen from the Fig. that, along the peak the flow velocity is higher in stream-wise direction compared to that in the trough (Rostamzadeh *et al*. 2014) . Because of this momentum difference, flow from the peak has a tendency to move towards trough as the flow progresses and that constitutes a span-wise flow from peak to trough.

From the Fig. 21 it can be noted that the pressure over the peaks is greater than in the troughs. As a result, there is strong adverse pressure gradient in the troughs than that over the peaks, that may lead to premature separation as is evident in C_p plots and surface streamline patterns.

The chord length varies continuously along the span between two consecutive peaks for the tubercled airfoil. As a result, Re based on chord also varies. Increase in Re makes the LSB to move downstream of the flow (Lyon *et al*. 1997). In case of an airfoil with tubercle, the Re is highest at the peak and gradually reduces to the lowest at the trough and increases again until the next peak is reached. Consequently, in the region between the peak and trough, the LSB starts to move towards the leading edge and in the region between trough and next peak, in the downstream direction. This results in the formation of LSB in a wavy-manner. The span-wise flow from peak to trough as well as the formation of counter-vortices in the region between peak and trough, contribute to higher momentum exchange rate that results in reduced bubble size as described in the previous section.

4. CONCLUSION

The aerodynamic performance of tubercled airfoil was tested numerically using $\gamma-Re_\theta$ transitional SST model at a low Re of 100,000. The Re was chosen to be close to the operational condition of a SSWT and consequently, the thin airfoil E216 suitable for low Re application was selected. Simulation results reveal that the tubercles enhance the lift marginally, simultaneously increasing the drag in the pre-stall region. Smaller tubercle amplitude led to gentle stall.

Tubercles significantly affected the surface pressure distribution on the airfoil and associated flow characteristics. In most of the cases, suction peak pressure became higher along the trough and lower along the peak, the difference being higher for larger tubercle wavelength. In general, the tubercles considerably reduced the height and width of LSB, complete elimination of LSB was observed for smaller amplitude and wavelength. The results indicate that the tubercled wind turbine blades could help overcome the laminar separation problem faced by SSWT, could increase the electrical power generation by maintaining power production during stall conditions. Increasing amplitude and wavelength made the

LSB to move slightly towards leading edge. The LSB is formed at different stream-wise locations behind trough and peak inducing three-dimensional wavy LSB unlike straight as in baseline. Unlike the previous studies, two pairs of counter vortices are formed on the airfoil surface in the region between the peak and trough of the tubercle at different chord-wise locations.

ACKNOWLEDGMENT

Authors would like to acknowledge the financial support extended by the Science & Engineering Research Board (SERB), India (Order No.: EMR/2015/000879) to carry out this research work.

REFERENCES

Arai, H., Y. Doi, T. Nakashima and H. Mutsuda (2010). A study on stall delay by various wavy leading edges. *Journal of aero aqua bio-mechanisms* 1(1), 18–23.

Bolzon, M. D., R. M. Kelso and M. Arjomandi (2015). Tubercles and their applications. *Journal of Aerospace Engineering* 29(1), 04015013.

Bolzon, M. D., R. M. Kelso and M. Arjomandi (2016). Formation of vortices on a tubercled wing, and their effects on drag. *Aerospace Science and Technology* 56, 46–55.

Bolzon, M. D., R. M. Kelso and M. Arjomandi (2017a). Force measurements and wake surveys of a swept tubercled wing. *Journal of Aerospace Engineering* 30(3), 04016085.

Bolzon, M. D., R. M. Kelso and M. Arjomandi (2017b). Performance effects of a single tubercle terminating at a swept wing's tip. *Experimental Thermal and Fluid Science* 85, 52–68.

Bushnell, D. M. and K. Moore (1991). Drag reduction in nature. *Annual Review of Fluid Mechanics* 23(1), 65–79.

Cai, C., Z. Zuo, S. Liu and Y. Wu (2015). Numerical investigations of hydrodynamic performance of hydrofoils with leading-edge protuberances. *Advances in Mechanical Engineering* 7(7), 1687814015592088.

Cai, C., Z. Zuo, T. Maeda, Y. Kamada, Q. Li, K. Shimamoto and S. Liu (2017). Periodic and aperiodic flow patterns around an airfoil with leading-edge protuberances. *Physics of fluids* 29(11), 115110.

Carreira Pedro, H. and M. Kobayashi (2008). Numerical study of stall delay on humpback whale flippers. In *46th AIAA aerospace sciences meeting and exhibit*, pp. 584.

Chishty, M. A., K. Parvez, S. Ahmed, H. R. Hamdani and A. Mushtaq (2011). Transition prediction in low pressure turbine (lpt) using gamma theta model and passive control of separation. In *ASME 2011 International Mechanical Engineering Congress and Exposition*, pp. 193–200. American Society of Mechanical Engineers Digital Collection.

Crivellini, A., V. D'Alessandro, D. Di Benedetto, S. Montelpare and R. Ricci (2014). Study of laminar separation bubble on low reynolds number operating airfoils: Rans modelling by means of an high-accuracy solver and experimental verification. In *Journal of Physics: Conference Series*, Volume 501, pp. 012024. IOP Publishing.

Custodio, D. S. (2007). The effect of humpback whale-like protuberances on hydrofoil performance.

de Paula, A. A., J. Meneghini, V. G. Kleine and R. D. Girardi (2017). The wavy leading edge performance for a very thick airfoil. In *55th AIAA Aerospace Sciences Meeting*, pp. 0492.

Fagbenro, K., M. Mohamed and D. Wood (2014). Computational modeling of the aerodynamics of windmill blades at high solidity. *Energy for Sustainable Development* 22, 13– 20.

Favier, J., A. Pinelli and U. Piomelli (2012). Control of the separated flow around an airfoil using a wavy leading edge inspired by humpback whale flippers. *Comptes Rendus Mecanique* 340(1-2), 107–114.

Filho, G. B., A. L. Da Costa, A. A. de Paula and G. R. De Lima (2018). A numerical investigation of the wavy leading edge phenomena at transonic regime. In *2018 AIAA Aerospace Sciences Meeting*, pp. 0317.

Fish, F. E. and J. M. Battle (1995). Hydrodynamic design of the humpback whale flipper. *Journal of Morphology* 225(1), 51–60.

FLUENT (2014). 15.0. *Theory Guide*.

Genc, M. S., I. Karasu, H. H. Acikel, M. T. Akpolat and M. Genc (2012). Low reynolds number flows and transition. *Low Reynolds Number Aerodynamics and Transition, Genc, MS Ed.; InTech: Rijeka, Croatia*, 1–28.

Godard, G. and M. Stanislas (2006). Control of a decelerating boundary layer. part 1: Optimization of passive vortex generators. *Aerospace Science and Technology* 10(3), 181–191.

Hansen, K. L. (2012). *Effect of leading edge tubercles on airfoil performance.* Ph. D. thesis.

Hansen, K. L., R. M. Kelso and B. B. Dally (2011). Performance variations of leadingedge tubercles for distinct airfoil profiles. *AIAA journal* 49(1), 185–194.

Hansen, K. L., N. Rostamzadeh, R. M. Kelso and B. B. Dally (2016). Evolution of the streamwise vortices generated between leading edge tubercles. *Journal of Fluid Mechanics 788*, 730–766.

Hu, H. and Z. Yang (2008). An experimental study of the laminar flow separation on a low-reynolds-number airfoil. *Journal of Fluids Engineering* 130(5), 051101.

Johari, H., C. W. Henoch, D. Custodio and A. Levshin (2007). Effects of leading-edge protuberances on airfoil performance. *AIAA Journal* 45(11), 2634–2642.

Lu, Y., Z. Li, X. Chang, Z. Chuang and J. Xing (2021). An aerodynamic optimization design study on the bio-inspired airfoil with leading-edge tubercles. *Engineering Applications of Computational Fluid Mechanics* 15(1), 293–313.

Lyon, C., M. Selig, A. Broeren, C. Lyon, M. Selig and A. Broeren (1997). Boundary layer trips on airfoils at low Reynolds numbers. In *35th Aerospace Sciences Meeting and Exhibit*, pp. 511.

Menter, F., R. Langtry and S. Völker (2006a). Transition modelling for general purpose cfd codes. *Flow, turbulence and combustion* 77(1-4), 277–303.

Menter, F. R., R. B. Langtry, S. Likki, Y. Suzen, P. Huang and S. Völker (2006b). A correlation-based transition model using local variables—part i: model formulation. *Journal of turbomachinery* 128(3), 413–422.

Miklosovic, D., M. Murray, L. Howle and F. Fish (2004). Leading-edge tubercles delay stall on

humpback whale (megaptera novaeangliae) flippers. *Physics of Fluids* 16(5), L39–L42.

Miklosovic, D. S., M. M. Murray, and L. E. Howle (2007). Experimental evaluation of sinusoidal leading edges. *Journal of Aircraft 44*(4), 1404–1408.

Musial, W. and D. Cromack (1988). Influence of reynolds number on performance modeling of horizontal axis wind rotors. *Journal of Solar Energy Engineering* 110(2), 139–144.

Ozen, C. and D. Rockwell (2010). Control of vortical structures on a flapping wing via a sinusoidal leading-edge. *Physics of fluids* 22(2), 021701.

Rahimi, H., W. Medjroubi, B. Stoevesandt and J. Peinke (2014). 2d numerical investigation of the laminar and turbulent flow over different airfoils using openfoam. In *Journal of Physics: Conference Series*, Volume 555, pp. 012070. IOP Publishing.

Rostamzadeh, N., K. Hansen, R. Kelso and B. Dally (2014). The formation mechanism and impact of streamwise vortices on naca 0021 airfoil's performance with undulating leading edge modification. *Physics of Fluids 26*(10), 107101.

Rostamzadeh, N., R. Kelso, B. Dall and K. Hansen (2013). The effect of undulating leading-edge modifications on naca 0021 airfoil characteristics. *Physics of fluids 25*(11), 117101.

Serson, D. and J. Meneghini (2015). Numerical study of wings with wavy leading and trailing edges. *Procedia Iutam* 14, 563–569.

Serson, D., J. Meneghini and S. Sherwin (2017). Direct numerical simulations of the flow around wings with spanwise waviness at a very low Reynolds number. *Computers & Fluids* 146, 117–124.

Shah, H., S. Mathew and C. M. Lim (2015). Numerical simulation of flow over an airfoil for small wind turbines using the γ-Re_θ model. *International Journal of Energy and Environmental Engineering* 6(4), 419–429.

Sheikholeslami, M. and D. Domiri Ganji (2017). Turbulent heat transfer enhancement in an air-to-water heat exchanger. *Proceedings of the Institution of Mechanical Engineers, Part E: Journal of Process Mechanical Engineering 231*(6), 1235–1248.

Skillen, A., A. Revell, A. Pinelli, U. Piomelli and J. Favier (2015). Flow over a wing with leading-edge undulations. *Aiaa Journal* 53(2), 464–472.

Sreejith, B. and A. Sathyabhama (2018). Numerical study on effect of boundary layer trips on aerodynamic performance of e216 airfoil. *Engineering science and technology, an international Journal* 21(1), 77–88.

Sreejith, B. and A. Sathyabhama (2020). Experimental and numerical study of laminar separation bubble formation on low Reynolds number airfoil with leading-edge tubercles. *Journal of the Brazilian Society of Mechanical Sciences and Engineering* 42(4), 1–15.

Stanway, M. J. (2008). *Hydrodynamic effects of leading-edge tubercles on control surfaces and in flapping foil propulsion*. Ph. D. thesis, Massachusetts Institute of Technology.

Stark, C., W. Shi and M. Atlar (2021). A numerical investigation into the influence of bio-inspired leading-edge tubercles on the hydrodynamic performance of a benchmark ducted propeller. *Ocean Engineering* 237, 109593.

Stein, B. and M. Murray (2005). Stall mechanism analysis of humpback whale flipper models. *Proceedings of Unmanned Untethered Submersible Technology (UUST), UUST05 5*.

Sudhakar, S., N. Karthikeyan and P. Suriyanarayanan (2019). Experimental studies on the effect of leading-edge tubercles on laminar separation bubble. *AIAA Journal* 57(12), 5197–5207.

Van Nierop, E. A., S. Alben, and M. P. Brenner (2008). How bumps on whale flippers delay stall: an aerodynamic model. *Physical Review Letters 100*(5), 054502.

Watts, P. and F. E. Fish (2001). The influence of passive, leading edge tubercles on wing performance. In *Proc. Twelfth Intl. Symp. Unmanned Untethered Submers. Technol*. Auton. Undersea Syst. Inst. Durham New Hampshire.

Weber, P. W., L. E. Howle, M. M. Murray and D. S. Miklosovic (2011). Computational evaluation of the performance of lifting surfaces with leading-edge protuberances. *Journal of Aircraft* 48(2), 591–600.

Wei, Z., T. New and Y. Cui (2015). An experimental study on flow separation control of hydrofoils with leading-edge tubercles at low reynolds number. *Ocean Engineering* 108, 336–349.

Wei, Z.,T. H. New and Y. Cui (2018). Aerodynamic performance and surface flow structures of leading-edge tubercled tapered swept-back wings. *AIAA Journal* 56(1), 423–431.

Wei, Z., J. Toh, I. Ibrahim and Y. Zhang (2019). Aerodynamic characteristics and surface flow structures of moderate aspectratio leading-edge tubercled wings. *European Journal of Mechanics-B/Fluids* 75, 143–152.

Zhang, M. and A. Frendi (2016). Effect of airfoil leading edge waviness on flow structures and noise. *International Journal of Numerical Methods for Heat & Fluid Flow*